Aerosol fabrication of thermosensitive nanogels and in situ hybridization with iron nanoparticles

Jeong Hoon Byeon and Jang-Woo Kim

Related Articles

Positioning of nanometer-sized particles on flat surfaces by direct deposition from the gas phase
Appl. Phys. Lett. 78, 3708 (2001)
Submicron-sized spherical yttrium oxide based phosphors prepared by supercritical CO2-assisted aerosolization and pyrolysis
Appl. Phys. Lett. 71, 1643 (1997)
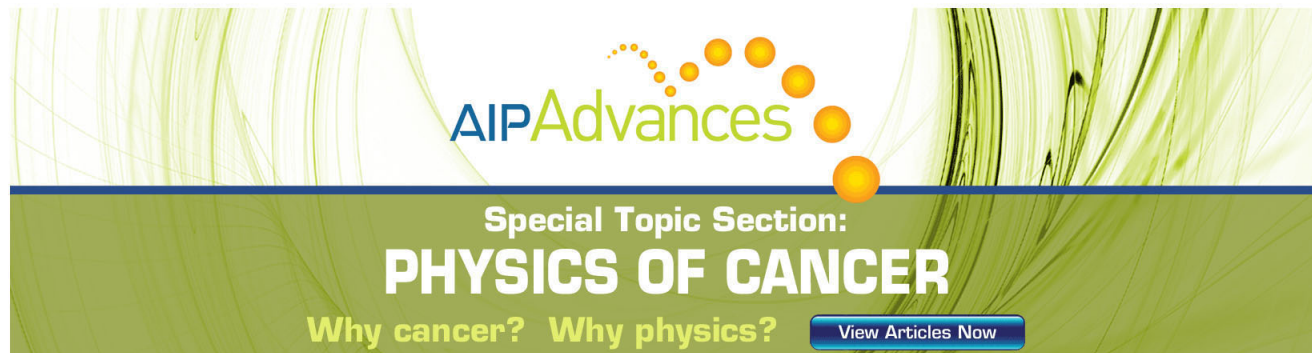
Additional information on Appl. Phys. Lett.

Aerosol fabrication of thermosensitive nanogels and *in situ* hybridization with iron nanoparticles

Jeong Hoon Byeon[1] and Jang-Woo Kim[2,a]

[1]*Department of Chemistry, Purdue University, West Lafayette, Indiana 47907, USA*
[2]*Department of Digital Display Engineering, Hoseo University, Asan 336-795, South Korea*

Collison atomized *n*-isopropylacrylamide (NIPAM) droplets were thermally treated with different furnace wall temperatures to form nanogels in an aerosol state. The size of the aerosol nanogels decreased from 40.3 nm to 32.8 nm by increasing the temperature from 40 °C to 90 °C due to the coil-to-globule transition of the NIPAM. A serial reactor consisting of a spark generator coupled to a collison atomizer was further employed to efficiently (>90% in production yield) fabricate biocompatible (78.8% in cell viability)-magnetic (30.3 emu g^{-1} in saturation magnetization) hybrid nanogels of NIPAM and iron nanoparticles. © *2012 American Institute of Physics.* [http://dx.doi.org/10.1063/1.4736574]

The synthesis of thermosensitive nanogels has attracted extensive interest because of their great potential applications in biomedical, electronic, and optical materials as well as in catalysis.[1] Of the materials, *N*-isopropylacrylamide (NIPAM) has a low critical solution temperature around 32 °C; it dissolves in water below this temperature and precipitates from the solution above this temperature due to the disruption of the hydrogen bonding with water and the increasing hydrophobic interactions among isopropyl groups.[2]

In recent decades, NIPAM has been combined with inorganic components, such as quantum dot, silver, gold, or magnetic nanoparticles, to yield nanostructured and multifunctional hybrid materials.[1,3–6] Depending on the inorganic nanoparticles used, the resultant hybrid nanogels can have various special properties, such as fluorescence, local surface plasmons, magnetic properties, etc. In order to develop hybrid nanogels with specific properties, specific synthetic methods need to be explored.

Many NIPAM-based nanogel systems exist as colloidal liquids (mostly conducted using time-consuming batch wet chemical processes) with the presence of chemical cross-linkers,[1] which are generally stable for short periods of time. However, some of these systems are designed to be gradually degradable by hydrolysis, so long-term storage in liquid form is not a viable option for these types of systems.[7,8] One method to overcome the stability limitations of storing liquid formulations is to dry the formulation, allowing storage in a powder form. In contrast to classical wet chemical methods, aerosol processing involves a much more limited number of preparation steps. It also produces material continuously, allows for a straightforward collection of particles and generates low waste.[9]

The purpose of the present work is to fabricate thermosensitive nanogels using a one-step aerosol method and explore the effects of heat treatment on their size and morphology. NIPAM was first dissolved in deionized water, then aerosolized, and finally thermally treated. In order to further

fabricate hybrid nanogels, NIPAM was *in situ* hybridized with iron nanoparticles in an aerosol state.

In Fig. 1(a), a nitrogen (>99.99% purity) flow, which was controlled by a mass flow controller (Tylan, US), had a flow rate of 3 L min^{-1} and was used as the operating gas for atomizing a solution containing NIPAM (0.5–2.0 g, 99.0%, Acros Organics, US) dissolved in 100 mL of deionized water. The droplets then passed through a heated tubular flow reactor (GTF12/25/364, Lenton Furnaces, UK) operating at a 40–90 °C wall temperature to drive water from the droplets. The condition for complete evaporation could be estimated by considering the time required for the evaporation of the droplets and comparing it with the appropriate residence time in the tubular flow reactor. The characteristic time to saturate the gas with vapor from evaporating droplets, τ_d, is given *via* the equation

$$\tau_d = \frac{1}{2\pi D_d \delta_v C_n(D_d)},\qquad(1)$$

where D_d, δ_v, and $C_n(D_d)$ are the droplet diameter, vapor diffusion coefficient, and the droplet number concentration, respectively. The estimated and applied residence times were 16.8 and 17.6 s, respectively, which implies that experimental conditions were sufficient to drive off all of the solvent completely. Figure 1(b) shows the computed (Fluent 6.3, Ansys, US) velocity and temperature contours of the NIPAM aerosol flow in the tube furnace. The results revealed that the temperature of the flow was high (40–80 °C) in the wall area of the reactor, and it became lower (30–60 °C) when the gas passed through the tube to the outlet, although the velocity showed no significant differences between the temperature conditions. The flow temperature was lower than the glass transition temperature of NIPAM (∼135 °C), and consequently, the particles were not softened and the mechanical strength was sustained.[10]

Figure 2(a) shows the size distributions of the NIPAM aerosol nanoparticles with different furnace temperatures measured using the scanning mobility particle sizer (SMPS, TSI 3936, US; 4.6–163 nm detection range). The ranges of the number concentration (TNC), geometric mean diameter

a)Author to whom correspondence should be addressed. Electronic mail: jwkim@hoseo.edu.
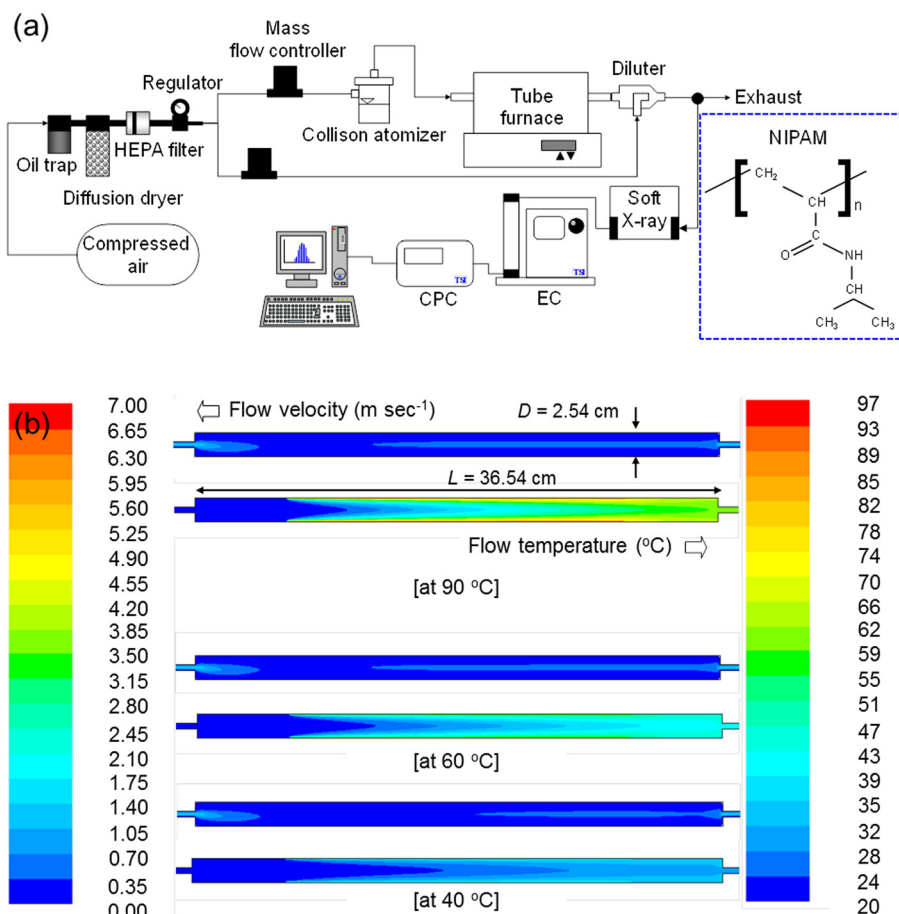
101, 023117-1

FIG. 1. (a) Schematic of NIPAM aerosol generation and subsequent heat treatment. (b) Computed velocity and temperature contours of NIPAM aerosol flow in the tube furnace.

(GMD), and geometric standard deviation (GSD) of the particles were $2.66\text{--}3.73 \times 10^5$ particles cm^{-3}, 32.8–40.3 nm, and 1.55–1.61, respectively. The different temperatures were probably represented by different size distributions, in accordance with the following equations:

$$\alpha = \frac{V_p(T)}{V_{p0}} \propto \left(\frac{D_p(T)}{D_{p0}}\right)^3, \tag{2}$$

$$N \propto k_g \left(\frac{D_p}{\alpha D_{p0}}\right)^{d_f}, \tag{3}$$

where α is the size reduction parameter, $V_p(T)$ (or $D_p(T)$) and V_{p0} (or D_{p0}) are the volumes (or diameters) of the NIPAM particles at temperature T and in the fully swollen state, respectively,[11] N is the number of agglomerates, k_g is the fractal prefactor, D_{p0} is the size of a primary NIPAM
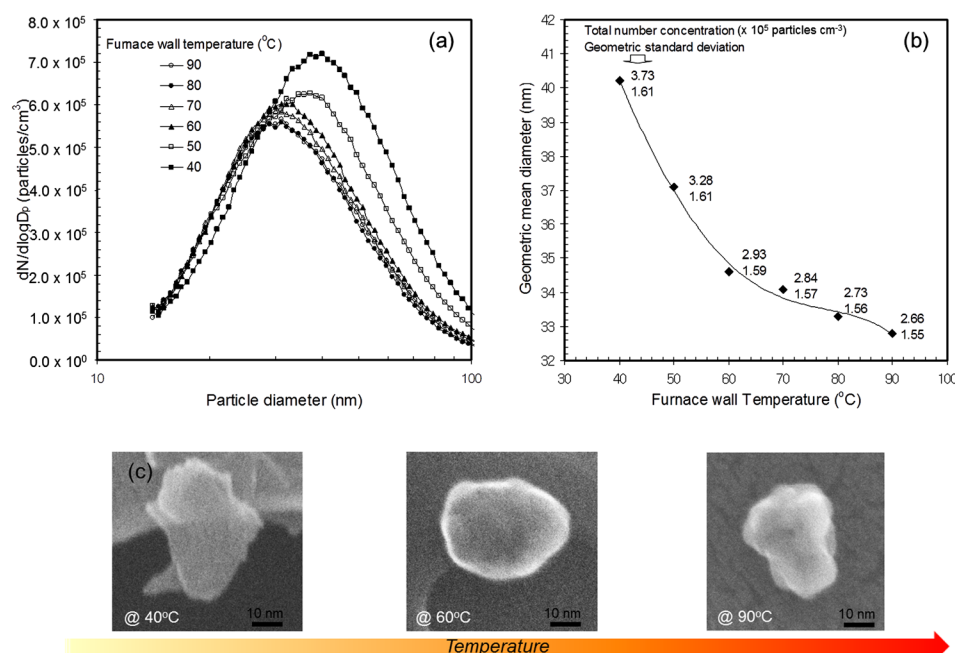

FIG. 2. Results for NIPAM aerosol nanoparticles. (a) Size distributions of NIPAM particles with different furnace wall temperatures. (b) Size distribution changes of NIPAM particles with increasing furnace temperature. (c) SEM images of NIPAM particles with increasing furnace temperature.

particle, and d_f is the fractal dimension. Although all the cases were operated at the same solution concentration of NIPAM, the concentrations and sizes of the measured aerosol particles varied according to the different degrees of shrinking (due to deswelling). The deswelling behavior of the particles is summarized in Fig. 2(b), where the size distribution of the particles obtained by the SMPS is plotted as a function of the wall temperature of the furnace. From this graph, the two different steps of particle reshaping, namely, agglomeration and shrinkage, were identified. Even though the size of the aerosol particles (also GSD) normally increased at a higher temperature by thermal collision [$K_{col} = \frac{4kT}{3\mu}$, where k is the Boltzmann factor and μ the gas viscosity], the particle size (also the GSD, from 1.61 to 1.55) decreased from 40.3 nm to 32.8 nm by the "coil-to-globule" transition.[12] From the scanning electron microscope (JSM-6500 F, JEOL, Japan) measurements, as shown in Fig. 2(c), the mean mode diameters for the 40 °C, 60 °C, and 90 °C cases were 44.1 ± 8.1, 38.8 ± 7.3, and 31.9 ± 6.6 nm, respectively, and these data were consistent with the data described in Fig. 2(b), which indicated that the heat treatment led to both a shrinkage in the particle morphology and a decrease in the particle size.

The size distributions of the NIPAM particles at different solution concentrations at a furnace temperature of 60 °C are presented in Fig. 3. The peak concentration of NIPAM aerosol particles increased from 3.73×10^5 to 7.07×10^5 particles cm^{-3} as the solution concentration of NIPAM increased from 0.5% to 2.0% (w/v). It also appears that the particle size varied with the NIPAM solution concentration; the size increased from 40.2 nm to 44.1 nm as the concentration increased. According to the regression result obtained from Fig. 3, there existed a relationship between the particle size and number, or $D_p \sim C_n^{0.14}$, where C_n is the particle number concentration.

A schematic of the system used for fabricating hybrid nanogels of NIPAM and iron nanoparticles is shown in Fig. 4(a). A spark discharge[13–15] produced an iron nanoparticle laden nitrogen flow which was used as the operating gas for atomizing the NIPAM solution. The iron nanoparticles passed over the atomizer orifice (0.3 mm diameter) where they mixed with atomized particles to form hybrid droplets (location 1). The droplets then passed through a heated tubular flow reactor operating at a 60 °C wall temperature to drive water from the droplets (location 2), resulting in hybrid nanogels (location 3). Figure 4(b) summarizes results of the hybrid nanogel fabrication. The TNC, GMD, and GSD of the nanogels are 2.80×10^6 particles cm^{-3}, 27.7 nm, and 1.90, respectively. The same data for individual iron particles are 1.12×10^7 particles cm^{-3}, 31.2 nm, and 1.59, respectively, and for the NIPAM particles are 1.20×10^6 particles cm^{-3}, 42.1 nm, and 1.59, respectively. A replacement of the size distribution after *in situ* hybridizing with iron particles is represented by deagglomeration (by setting the force acting on an agglomerate of size D_{pa} due to the sudden pressure change across an orifice in the collison atomizer) and is given by[16]

$$D_p = \beta \sqrt{\frac{D_{pa}H}{6\pi\Delta P\Theta^2}}, \qquad (4)$$

where β is the proportionality constant, H is the Hamaker constant, ΔP is the pressure difference between the front and the rear of an orifice, and Θ is the parameter controlling the maximum cohesive strength between constituting particles in an agglomerate. Iron agglomerates passed through the orifice, and the rapid changes in pressure, density, and velocity across the orifice produced an impulse capable of shattering the agglomerates. The hybrid nanogels were smaller than both the individual iron and NIPAM particles. The bushy extended structures that characterize the reactant iron particles have vanished, to be replaced by loop-like nanogels [Fig. 4(c), by transmission electron microscope (Libra 120, Carl Zeiss, Germany)], where shattered iron particles were locked up inside the loop-like network. The crosslinking points were probably formed *via* natural electrostatic positive charges[17] and/or interparticle termination of propagating radicals on the iron particles,[18] because there was no addition of chemical crosslinkers. As shown in Fig. 4(b), we can also clearly observe the infrared spectra (IFS 66/S, Bruker Optics, Germany) of the amide I band (1658 cm^{-1}, O=C-NH) and the amide II band (1537 cm^{-1}, N-H stretching). The presence of two bands at 1368 and 1386 cm^{-1} are associated with the deformation of two methyl groups on isopropyl (-CH(CH$_3$)$_2$).[19] After the NIPAM was hybridized with iron particles, there were no significant differences between the NIPAM and hybrid nanogels, while the specific peak of the amide and methyl groups was intensified. This implies that the hybridization may generate a linkage between the iron particles and NIPAM molecules. In addition, the production yield of the hybrid nanogels was approximately 93%, and the yield was determined by the area fraction of the nanogels-to-all particles in the TEM image. The nanogels had a saturation magnetization (7404, Lake Shore Cryotronics, US) value of approximately 30.3 emu g^{-1}, indicating that the nanogels conserved superparamagnetic behavior. The cytotoxicity of the nanogel/plasmid deoxyribonucleic acid complexes was evaluated by MTS, 3-(4,5-dimethyl-thiazol-2-yl)-5-(3-carboxymethoxyphenyl)-2-(4-sulfophenyl)2H-tetrazolium, assay in human embryonic kidney 293 cells. The results
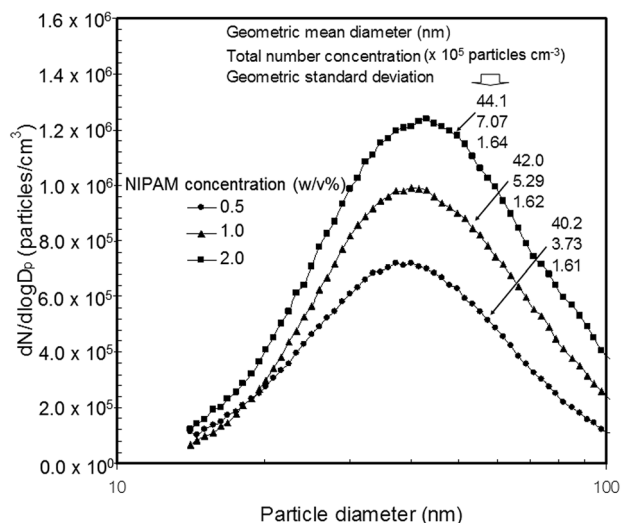

FIG. 3. Size distributions of NIPAM aerosol particles with different NIPAM solution concentrations.
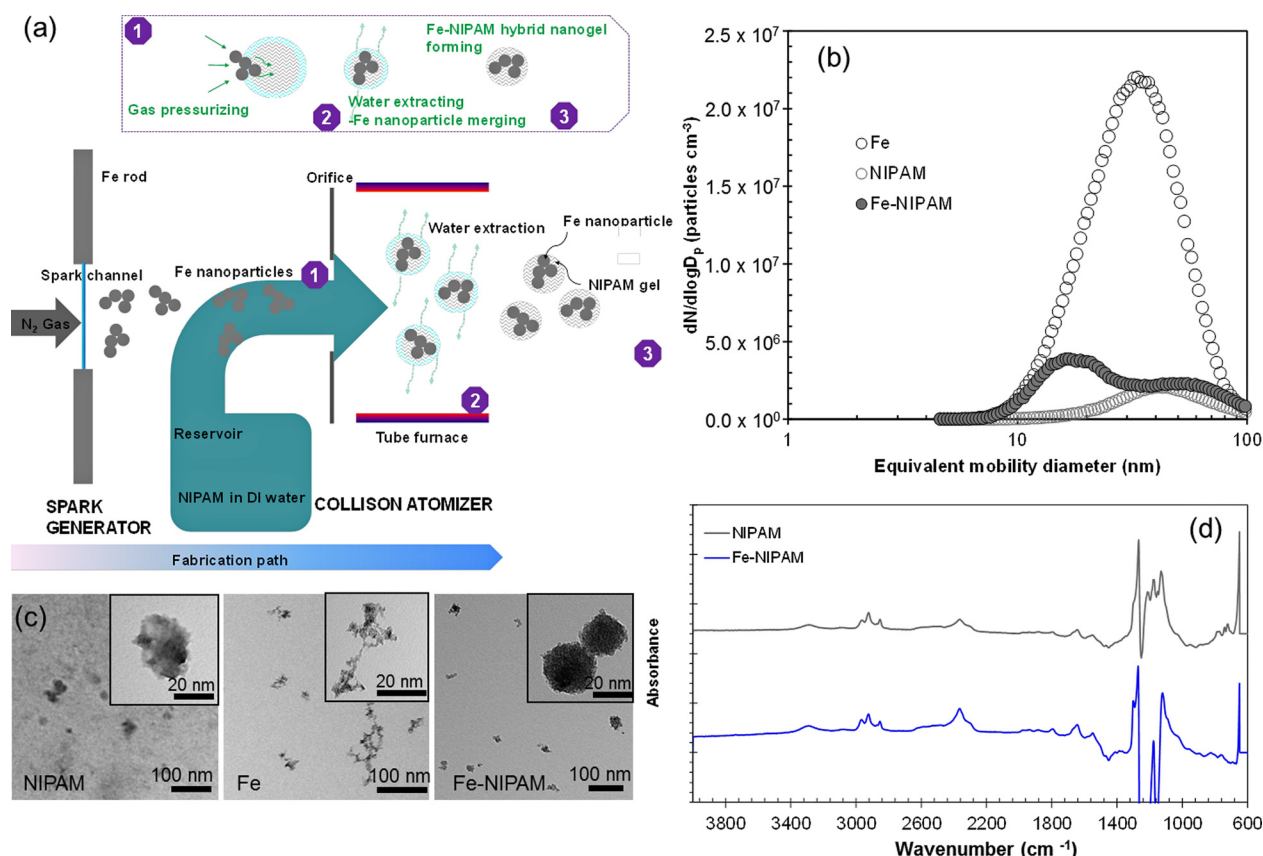
FIG. 4. Results for hybrid nanogels of NIPAM and iron nanoparticles. (a) *In situ* fabrication of the hybrid nanogels by a serial aerosol reactor consisting of a spark generator and a collison atomizer. (b) Size distributions of NIPAM, iron, and hybrid nanogel particles. (c) TEM images of NIPAM, iron, and hybrid nanogel particles. (d) FTIR spectra of NIPAM and hybrid nanogel particles.

show that the range of cell viability is about ∼80% for all the tested nanogels, and there are no significant differences between the storage days (5 days: 79.8%, 30 days: 79.7%, 90 days: 79.4%). This implies that the nanogels have biocompatibility and stability that may be suitable in a clinical context.

An aerosol-based method has been used to aerosol construct thermosensitive nanogels and for *in situ* hybridization with iron nanoparticles. Scale-up would depend on the rate of spark nanoparticle iron generation. The development of high iron number output systems may enhance production rate for the hybrid nanogel fabrication.[20] This method may provide a practical and relevant strategy for the controllable fabrication of various organic aerosols and their hybridized nanostructures and also provide opportunities to construct future organic-based materials and devices.

[1]T. Chen, Z. Cao, X. Guo, J. Nie, J. Xu, Z. Fan, and B. Du, Polymer **52**, 172 (2011).

[2]M. Temtem, T. Casimiro, J. F. Mano, and A. Aguiar-Ricardo, Green Chem. **9**, 75 (2007).

[3]Y.-Q. Wang, Y.-Y. Zhang, F. Zhang, and W.-Y. Li, J. Mater. Chem. **21**, 6556 (2011).

[4]A. Murugadoss, A. Khan, and A. Chattopadhyay, J. Nanopart. Res. **12**, 1331 (2010).

[5]T. Wu, Z. Ge, and S. Liu, Chem. Mater. **23**, 2370 (2011).

[6]M. Laurenti, P. Guardia, R. Contreras-Cáceres, J. Pérez-Juste, A. Fernandez-Barbero, E. Lopez-Cabarcos, and J. Rubio-Retama, Langmuir **27**, 10484 (2011).

[7]J.-H. Park, Y.-H. Lee, and S.-G. Oh, Macromol. Chem. Phys. **208**, 2419 (2007).

[8]V. Bulmus, Y. Chan, Q. Nguyen, and H. L. Tran, Macromol. Biosci. **7**, 446 (2007).

[9]S. E. Pratsinis, AIChE J. **56**, 3028 (2010).

[10]R. G. Sousa, W. F. Magalhães, and R. F. S. Freitas, Polym. Degrad. Stab. **61**, 275 (1998).

[11]M. Karg and T. Hellweg, Curr. Opin. Colloid Interface Sci. **14**, 483 (2009).

[12]X. Lian, J. Jin, J. Tian, and H. Zhao, ACS Appl. Mater. Interfaces **2**, 2261 (2010).

[13]J. H. Byeon, J. H. Park, and J. Hwang, J. Aerosol. Sci. **39**, 888 (2008).

[14]J. H. Byeon, J. H. Park, K. Y. Yoon, and J. Hwang, Nanoscale **1**, 339 (2009).

[15]J. H. Byeon and J.-W. Kim, Appl. Phys. Lett. **96**, 153102 (2010).

[16]D. To, R. Dave, X. Yin, and S. Sundaresan, AIChE J. **55**, 2807 (2009).

[17]J. H. Byeon and J.-W. Kim, Langmuir **26**, 11928 (2010).

[18]M. Czaun, L. Hevesi, M. Takafuji, and H. Ihara, Chem. Commun. **18**, 2124 (2008).

[19]P. Li, A. M. Zhu, Q. L. Liu, and Q. G. Zhang, Ind. Eng. Chem. Res. **47**, 7700 (2008).

[20]J. H. Byeon and J. T. Roberts, ACS Appl. Mater. Interfaces **4**, 2693 (2012).